Available online at www.sciencedirect.com
ScienceDirect
Trans. Nonferrous Met. Soc. China 32(2022) 3914−3925
Transactions of Nonferrous Metals Society of China
www.tnmsc.cn

High specific strength MWCNTs/Mg−14Li−1Al composite prepared by electrophoretic deposition, friction stir processing and cold rolling

Lin XU[1], Jia-hao WANG[1], Rui-zhi WU[1,2], Chun-bo ZHANG[3], Hua-jie WU[1], Le-gan HOU[1], Jing-huai ZHANG[1]

1. Key Laboratory of Superlight Materials & Surface Technology, Ministry of Education, Harbin Engineering University, Harbin 150001, China;
2. College of Science, Heihe University, Heihe 164300, China;
3. Harbin Welding Institute Limited Company, Harbin 150001, China

Received 14 September 2021; accepted 20 April 2022

Abstract: Multi-wall carbon nanotubes reinforced Mg−14Li−1Al composite (MWCNTs/Mg−14Li−1Al) was prepared by the processes of electrophoretic deposition, friction stir processing, and cold rolling. The microstructure and mechanical properties of the composite were investigated. The results show that, the microhardness of the composite is up to HV 84.4, which is 91.38% higher than that of the as-cast matrix alloy (HV 44.1). The yield strength and ultimate tensile strength of the composite are 259 and 313 MPa, which are 135.45% and 115.86% higher than those of the as-cast matrix alloy, respectively, and a high specific strength of 221.98 kN·m/kg is obtained. In the composite, the MWCNTs serve as nucleation particles during the friction stir processing and cold rolling, causing dynamic recrystallization and grain refinement. Furthermore, MWCNTs hinder the movement of dislocations and transfer the load from the matrix alloy, thus improving the strength.

Key words: metal matrix composites; Mg−Li alloy; multi-wall carbon nanotubes; electrophoretic deposition; friction stir processing; rolling; strengthening mechanism

1 Introduction

Mg−Li alloy is the lightest metallic engineering material, with a density of 1.35−1.65 g/cm^3 [1,2]. It possesses the advantages of high specific strength [3], excellent damping property [4], and good electromagnetic shielding property, and so on [5]. However, this kind of alloy always possesses poor strength [6,7], which limits its wide applications.

The strength of Mg−Li matrix composite is always much higher than that of the corresponding Mg−Li alloy. Carbon nanotube has high strength and Young's modulus [8], which makes it become an ideal reinforcement in Mg-matrix composites. To uniformly disperse the reinforcement in the composites, electrophoretic deposition (EPD) is one of the most effective and promising methods, and it is widely used to graft multi-wall carbon nanotubes (MWCNTs) onto the surface of matrix alloy. EPD possesses the advantages of a negligible damage to MWCNTs, a high deposition density, and a uniform dispersion [9]. Friction stirring processing (FSP) is a kind of severe plastic deformation technology. During FSP, not only the dynamic recrystallization and refinement happen, but also the microstructure is effectively mixed and reconstructed, homogenized, and refined, thus improving the mechanical properties [10−12]. Accordingly, FSP can be used to process metal matrix composites. In the process of FSP, groove filling or hole filling is

Corresponding author: Rui-zhi WU, Tel/Fax: +86-451-82569890, E-mail: rzwu@hrbeu.edu.cn;
Le-gan HOU, Tel/Fax: +86-451-82569890, E-mail: houlegan@hrbeu.edu.cn
DOI: 10.1016/S1003-6326(22)66067-9

usually used to add reinforcements into the matrix alloy [13,14]. However, FSP processed composites often have some drawbacks, such as grain coarsening in the processed region and low dislocation density in the matrix alloy due to a large amount of generated heat [15]. To overcome these drawbacks, rolling can be used to further process the materials [16].

In this work, to improve the mechanical properties of Mg−14Li−1Al (LA141) alloy, LA141 alloy was used as matrix alloy and MWCNTs were used as reinforcement, and MWCNTs/Mg−14Li−1Al composite was prepared by EPD, FSP and cold rolling. The microstructure and mechanical properties of the prepared MWCNTs/Mg−14Li−1Al composite were analyzed and discussed.

2 Experimental

As-cast LA141 alloy was used as the matrix alloy in this work. MWCNTs, with a purity of 95 wt.%, an inner diameter of 3−5 nm, an outer diameter of 8−15 nm, and a length of 3−12 μm, were used as the reinforcement, as shown in Fig. 1(a). MWCNTs are entangled and agglomerated with each other.

Figure 2 shows the preparation process of MWCNTs/Mg−14Li−1Al composite. LA141 alloy was cut into plates with sizes of 110 mm × 40 mm × 14 mm, and they were named as Sample 1. Then, the plates were pre-rolled at 250 °C with a reduction of 10% in each pass with a final thickness of 2 mm, which were named as Sample 2. The rolled plates was cut into 150 mm × 115 mm × 2 mm plates, and some of the plates were electrophoretic deposition (EPD) processed to form MWCNTs films on the surface of them, then they were stacked and rolled; the other plates were directly stacked and rolled for comparison. In EPD, 2 g MWCNTs, 1.2 g $Al(NO_3)_3$, and 0.2 g polyvinylpyrrolidone (PVP) were dissolved into 2 L solution which is a mixture of anhydrous ethanol and acetone with a volume ratio of 1:1, then the solution was ultrasonically dispersed for 8 h to obtain an electrophoresis solution with a good suspension. Subsequently, EPD was carried out with the rolled LA141 alloy as the cathode and the stainless steel sheet with the same size as the anode

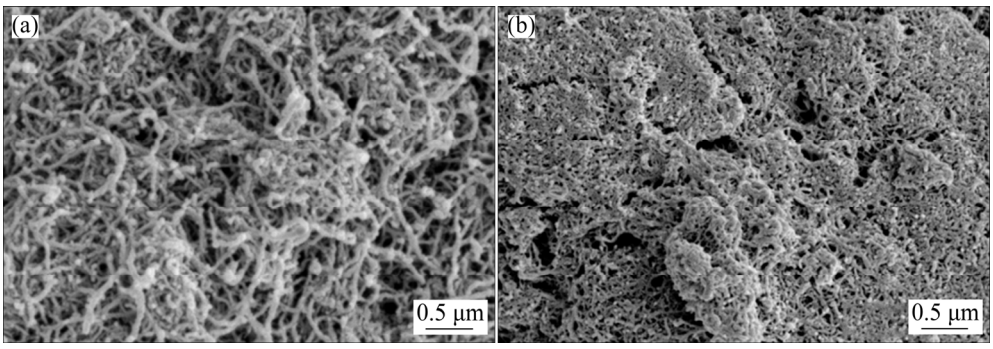

Fig. 1 SEM images of MWCNTs (a) and MWCNTs film (b)

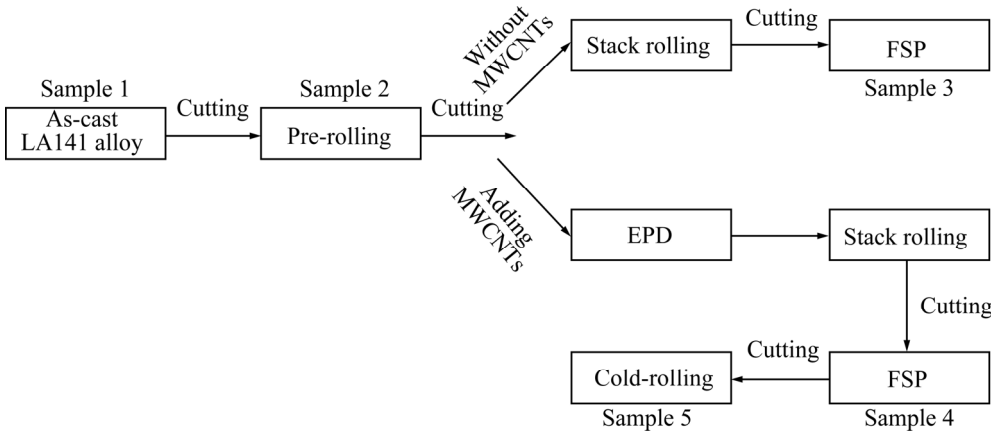

Fig. 2 Preparation process of MWCNTs/Mg−14Li−1Al composite

at a voltage of 30 V and a current of 0.5 A for 5 min. The deposited sample was naturally dried for 1 h. The obtained MWCNTs film is shown in Fig. 1(b). MWCNTs are deposited uniformly on the surface of LA141 by EPD. The plates with and without 0.8 wt.% MWCNTs were both stacked and heated at 300 °C for 30 min, then they were rolled from 14 to 5 mm with a reduction of 64%. The obtained plates were cut into 140 mm × 130 mm × 5 mm for subsequent FSP. The FSP-processed plate without MWCNTs was named as Sample 3 and the one with MWCNTs was named as Sample 4. In FSP, the FSP tool was composed of a circular shaft shoulder with a diameter of 18 mm and a threaded stirring pin with a diameter of 6 mm, and a length of 3 mm. The rotation speed and movement speed of the FSP tool were 900 r/min and 40 mm/min, respectively. The inclination angle was 2.5°. Some samples after FSP were cold-rolled (CR) at room temperature with a total reduction of 60%. The thickness of the cold-rolled sample was 2 mm, named as Sample 5.

The metallographic sample was mechanically polished and etched with a mixed solution of 4% nitric acid and 96% ethanol. The microstructure of the samples was observed using optical microscope (OM), scanning electron microscope (SEM), and transmission electron microscope (TEM). The average size of grains was measured by Nano Measurer 1.2 software. The density of the as-received composite was measured by a multifunctional solid density tester (HTY−300C). The tensile specimens were machined along the rolling direction (RD) and processing direction (PD) with dimensions of 48 mm × 8 mm × 2 mm. During tensile testing, the tensile speed was 1 mm/min. The microhardness was measured by a Vickers hardness tester with a load of 2 N and a dwelling time of 15 s.

3 Results

3.1 Microstructure

Figure 3 shows the OM images of the LA141 alloy in different states. Figure 4 shows the grain size distribution of the different samples. The as-cast LA141 alloy has relatively coarse grains with an average grain size of 280 μm, as shown in Fig. 3(a). After FSP, the grains of the alloy are refined. As shown in Fig. 3(b), without the addition of MWCNTs, the average size is 31 μm. As shown in Fig. 3(c), with the addition of MWCNTs, the average size is 16 μm. The grain size of the cold-

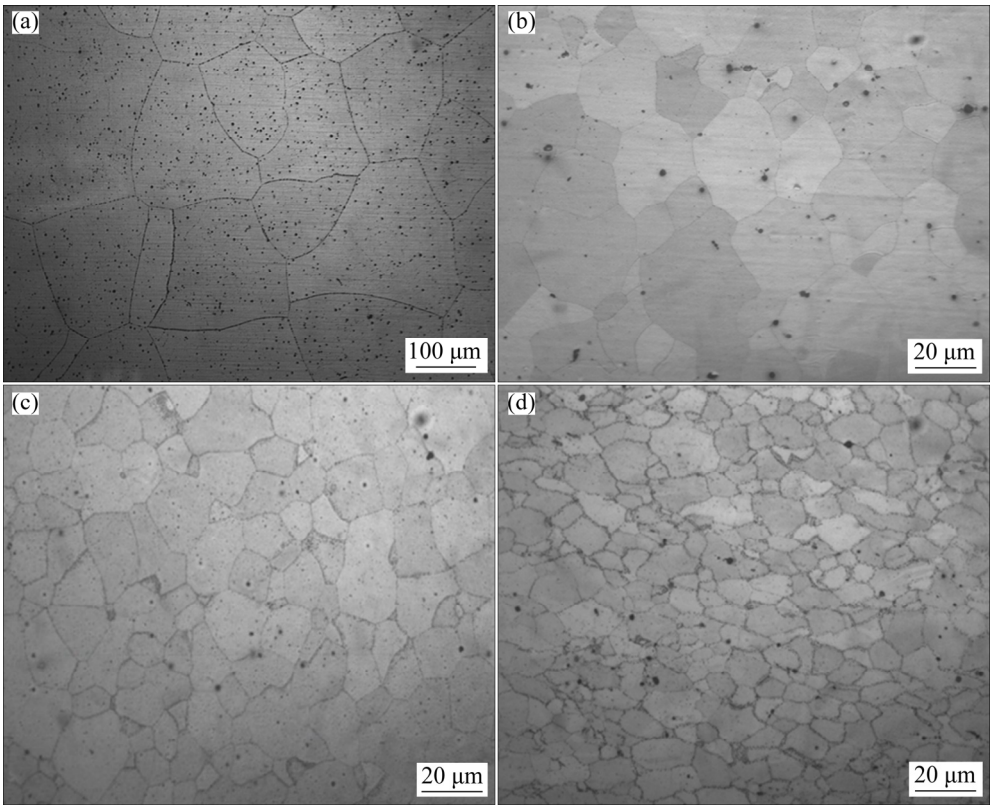

Fig. 3 OM images of different samples: (a) Sample 1; (b) Sample 3; (c) Sample 4; (d) Sample 5

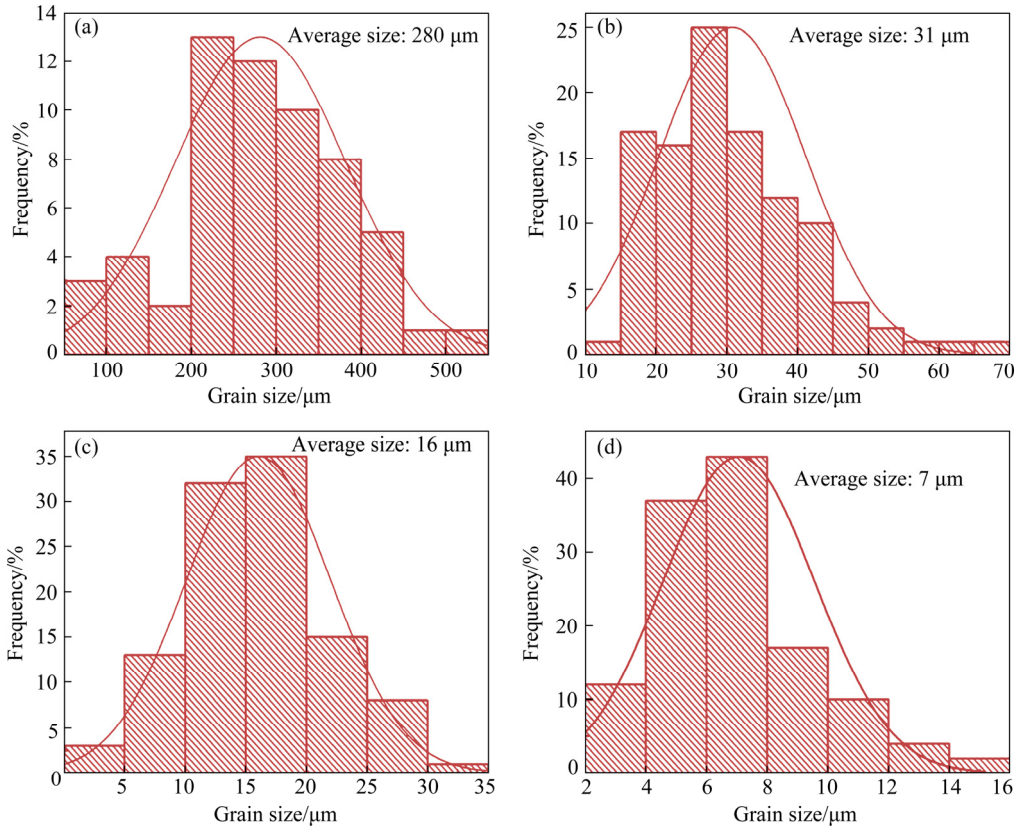

Fig. 4 Grain size distribution of different samples: (a) Sample 1; (b) Sample 3; (c) Sample 4; (d) Sample 5

rolled sample after FSP is the finest, with an average grain size of 7 μm. Compared with the as-cast alloy, the grains of cold-rolled sample after FSP are refined notably, showing obvious refining effects of MWCNTs, FSP, and cold-rolling.

The cross-section of the FSP-processed sample can always be divided into 4 zones: matrix, thermo-mechanical affected zone (TMAZ), heat-affected zone (HAZ) and nucleation zone (NZ), as shown in Fig. 5. However, HAZ does not appear in this sample. The grain size in NZ is finer than that in TMAZ because of the massive heat generated by the friction between the high-speed rotation tool and the matrix alloy, which leads to dynamic recrystallization in this zone, as shown in the solid rectangles in Figs. 6(a, c, e). However, fine grains and coarse grains both appear in NZ, showing a bimodal structure, which may be caused by incomplete recrystallization during FSP, as shown by the dotted circles in Figs. 6(a, b). After FSP, the agglomeration and nonuniform distribution of MWCNTs can be observed, but the grain size in TMAZ is significantly smaller than that without MWCNTs, as shown in Figs. 6(c, d). After rolling, the MWCNTs are uniformly dispersed in the matrix

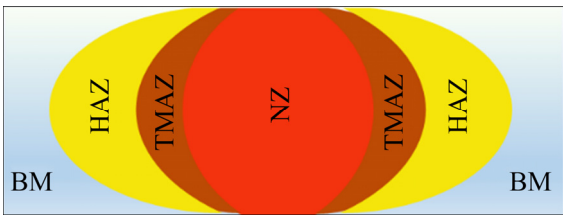

Fig. 5 Schematic diagram of different zones of friction stir processing

alloy, and the grain size becomes finer, compared with the FSP-processed samples, as shown in the solid rectangles in Fig. 6(e, f). This can be explained by the MWCNTs serving as the nucleation particles of the recrystallized grains and hindering the growth of the grains, resulting in a large number of fine recrystallized grains at the interface between NZ and TMAZ. In addition, after rolling, a mixed lamellar structure of MWCNTs and grains forms in the composite, and a mixed grain structure with fine and coarse grains also forms, as shown in Figs. 7(a, b). The formation of the lamellar structure may be caused by the dynamic recrystallization that occurs during the rolling process with MWCNTs as the nucleation particles.

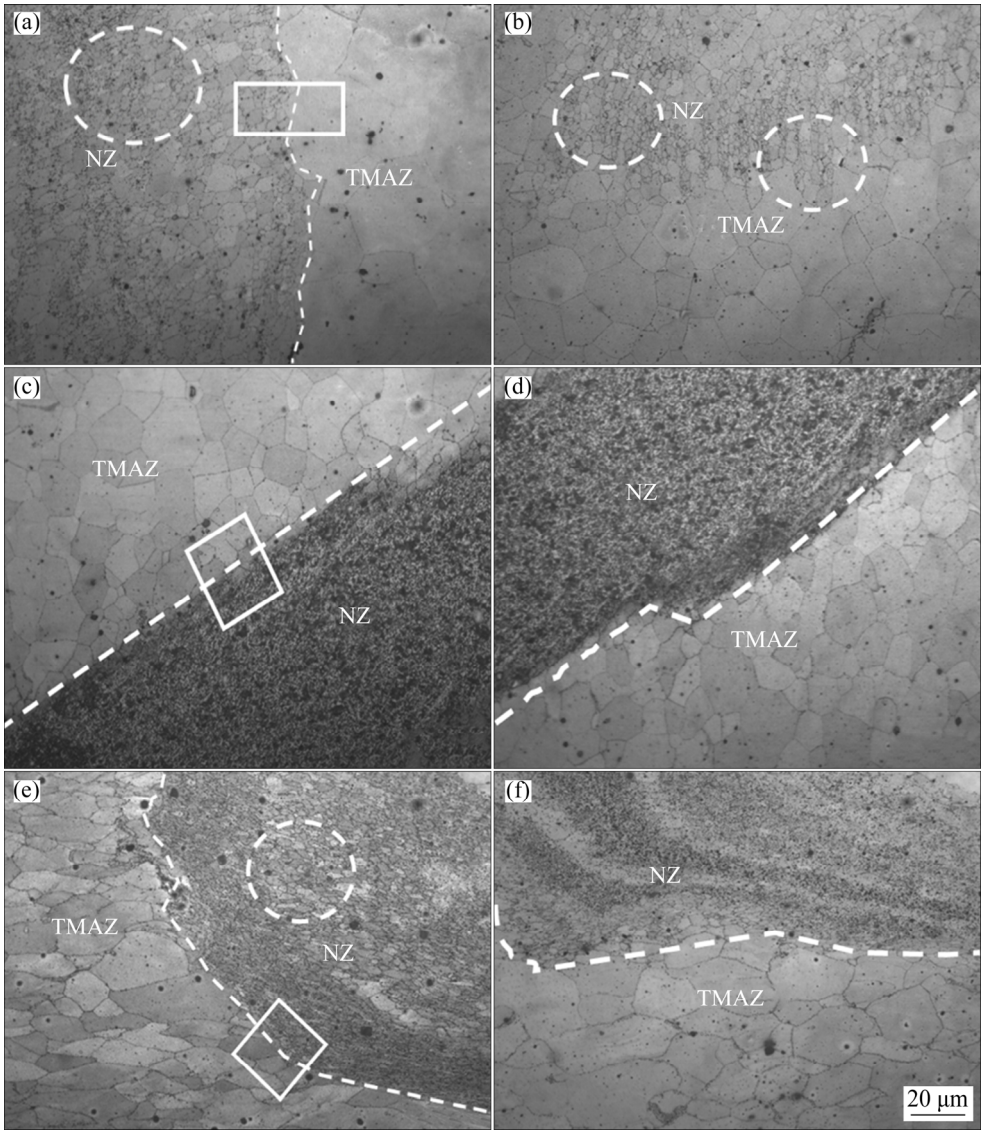

Fig. 6 OM images of stirring zone and heat-affected zone of different samples: (a, b) Sample 3; (c, d) Sample 4, (e, f) Sample 5

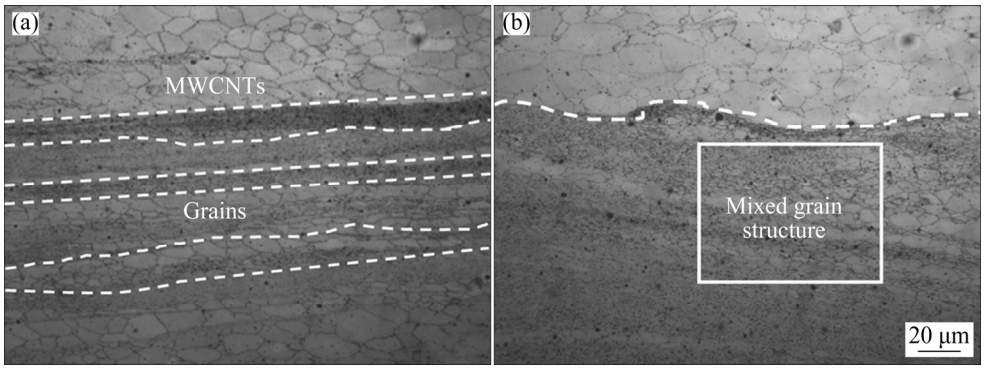

Fig. 7 OM images of Sample 5: (a) Lamellar structure; (b) Mixed grain structure

Figure 8 shows TEM images of the samples in different states. After FSP, some dislocations can be found in the FSP-processed Mg−14Li−1Al matrix alloy and MWCNTs/Mg−14Li−1Al composite, but the dislocation density is relatively small, as shown by the white arrows in Figs. 8(a, b). However, after

cold-rolling (CR), the dislocation density is higher than that of the FSP-processed sample, as shown by the white arrows in Fig. 8(c). After FSP and CR, some ultra-fine grains exist in the sample, as shown in the solid rectangles in Figs. 8(d−f). The ultra-fine grains in the sample after CR are finer and more numerous than those in the sample after FSP. Based on the OM results, the addition of MWCNTs is beneficial to grain nucleation and refinement. To confirm this conjecture, HAADF element scanning observation was performed on the LA141/MWCNTs composite, as shown in Fig. 9. The C element is uniformly distributed in the matrix alloy, indicating that MWCNTs are uniformly distributed in the composite, thus providing nucleation particles for grains, and refining the grains, as shown in Fig. 9(c). The tubular structure of MWCNTs can be clearly seen in the matrix alloy, as shown in the solid circle in Fig. 10(a), and there are a large number of ultra-fine grains around the MWCNTs, as shown in the solid rectangles in Fig. 10(a). Therefore, it is confirmed that the MWCNTs provide nucleation particles for recrystallized grains. The inset in Fig. 10(b) is the result of selected area

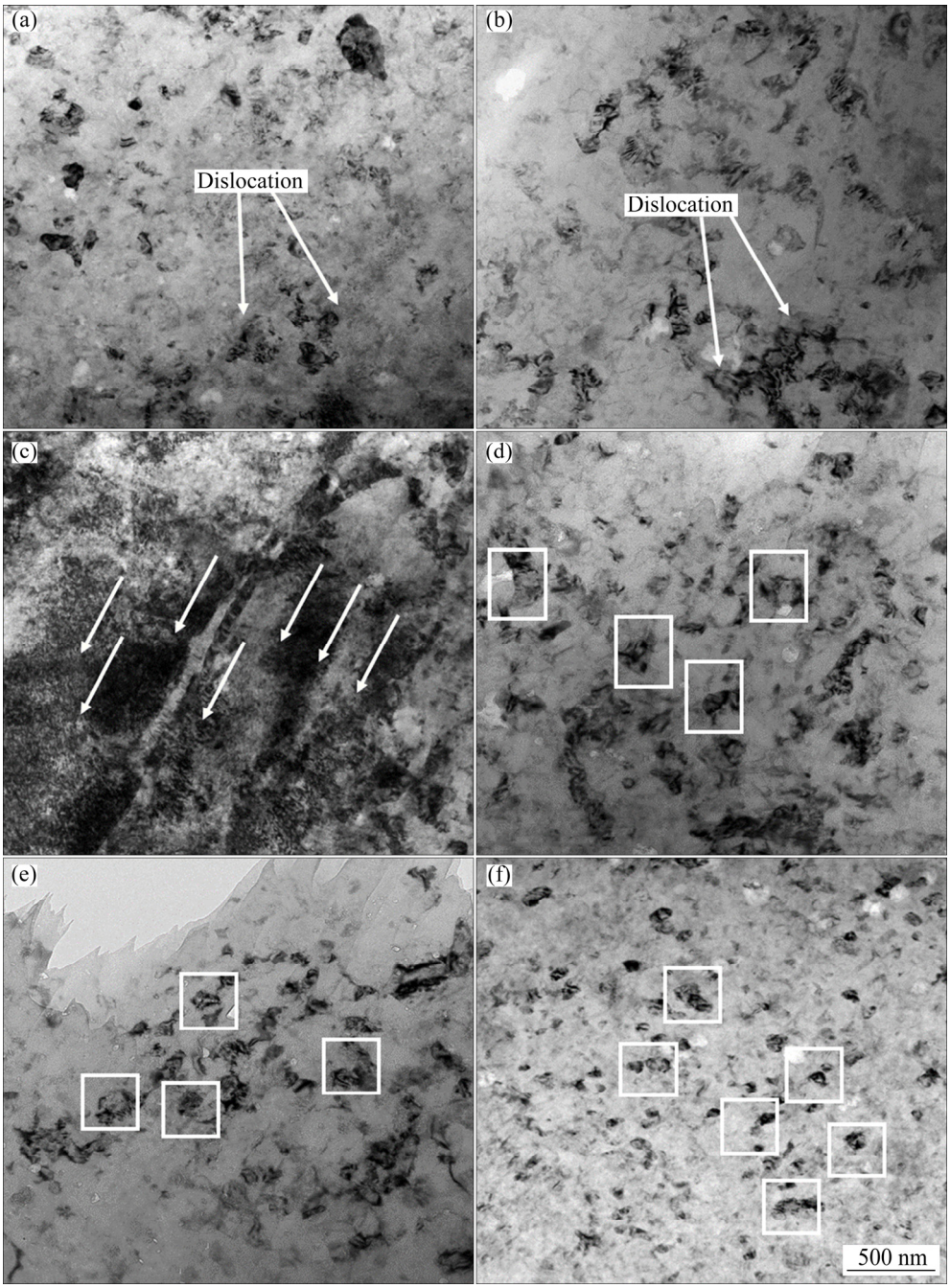

Fig. 8 TEM images of different samples: (a, d) Sample 3; (b, e) Sample 4; (c, f) Sample 5

electron diffraction (SAED) analysis, confirming the existence of MWCNTs. These results indicate that the presence of MWCNTs can effectively reduce the grain size.

3.2 Mechanical properties

The microhardness of the LA141 matrix alloy and composite in different states is shown in Fig. 11. After FSP and CR, the microhardness increases significantly. Sample 5 obtains the highest microhardness of HV 84.4, which is 91.38% higher than that of Sample 1 (HV 44.1) and 49.38% higher than that of Sample 2 (HV 56.5).

The engineering stress−strain curves of the LA141 matrix alloy and composite in different states are shown in Fig. 12. The ultimate tensile

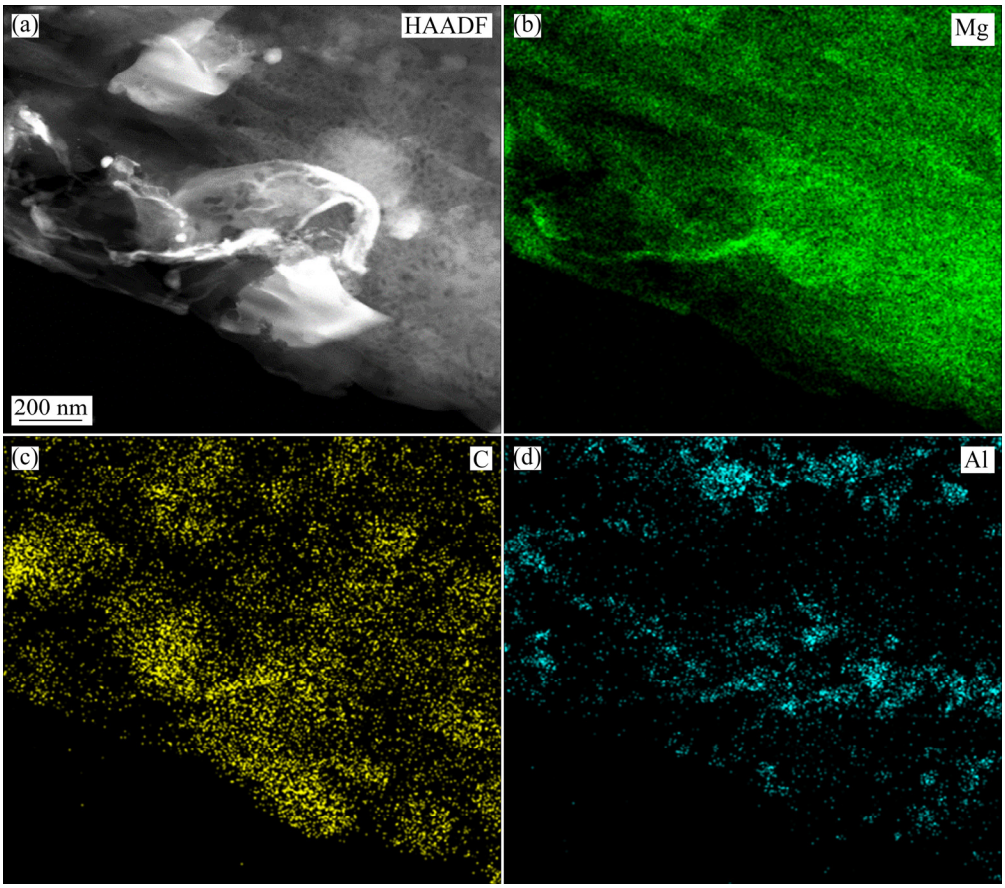

Fig. 9 TEM image (a) and corresponding HAADF element scan (b, c, d) of MWCNTs/Mg−14Li−1Al composite

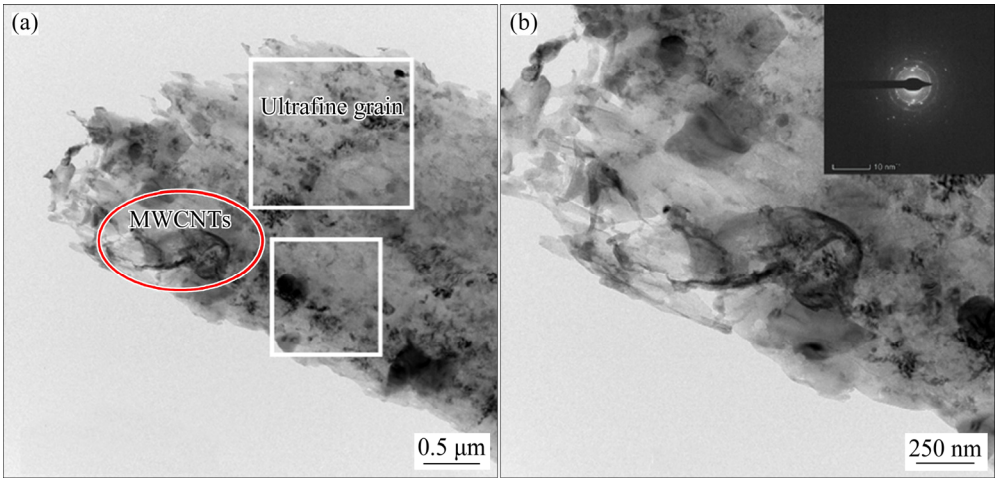

Fig. 10 TEM image of MWCNTs/Mg−14Li−1Al composite (a) and enlarged view of selected area (b) (Insert is SAED of MWCNTs)

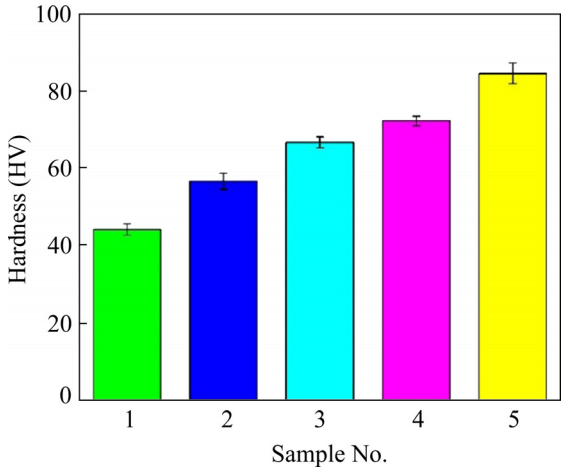

Fig. 11 Microhardness of different samples

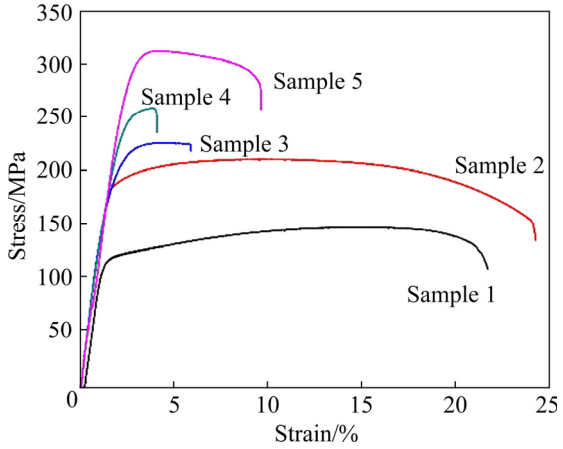

Fig. 12 Engineering stress−strain curves of different samples

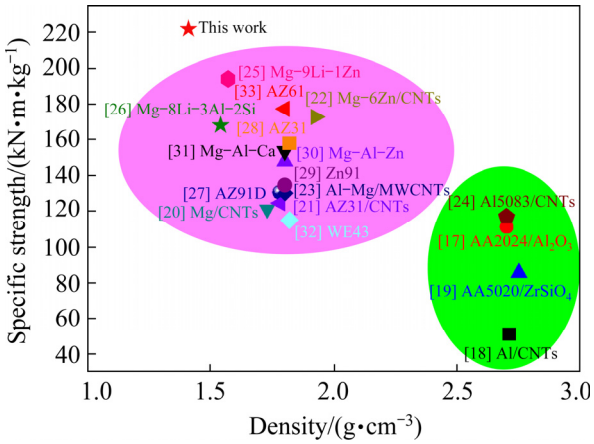

Fig. 13 Relationship between specific strength and density of different alloys

strength of the composite is greatly improved by FPS and CR. Sample 1 possesses the lowest strength, with the yield strength and ultimate tensile strength of 110 MPa and 145 MPa, respectively. Sample 2 possesses a yield strength of 176 MPa and ultimate tensile strength of 209 MPa. After FSP, the yield strength and ultimate tensile strength of Sample 3 are 213 MPa and 226 MPa, respectively. Compared with Sample 1, the yield strength and ultimate tensile strength of Sample 3 increase by 93.64% and 55.86%, respectively. Sample 4 possesses a yield strength of 234 MPa and ultimate tensile strength of 258 MPa, which are 112.73% and 77.93% higher than those of Sample 1. After CR, the mechanical properties of Sample 5 are significantly improved. The yield strength increases from 234 to 259 MPa, and the ultimate tensile strength increases from 258 to 313 MPa. Compared with Sample 1, the yield strength and ultimate tensile strength of Sample 5 increase by 135.45% and 115.86%, respectively.

Although the strength of Sample 5 is significantly improved, its elongation is lower than that of Samples 1 and 2. The elongation of Sample 4 is the lowest of all, only 4.07%. After CR, the elongation increases to 9.65%.

The density of the obtained MWCNTs/LA141 composite is 1.41 g/cm^3, and the specific strength of the MWCNTs/LA141 composite after CR is 221.98 kN·m/kg. Figure 13 shows the comparison of specific strength between this work and literature. It shows that the obtained MWCNTs/ LA141 composite possesses the lowest density and the highest specific strength.

4 Discussion

The grain refinement mechanism of the composite during FSP in this work can be expressed as Fig. 14. As a severe plastic deformation process, a large amount of heat is generated by the friction between the processing tool and the material, which provides energy for the dynamic crystallization of the matrix alloy, resulting in the formation of fine grains. In the FSP process, the material is subjected to the pressure (F) from the shoulder of the processing tool and the friction force (F_1) generated by the friction between the tool shoulder and the material during the moving process, but also the friction force F_2 and the shear force F_3 generated between the stirring pin and the material. Under F and F_1, a lot of heat is generated. The grains are broken and refined under F_2 and F_3. Because the stirring pin used in this study is threaded, the grains

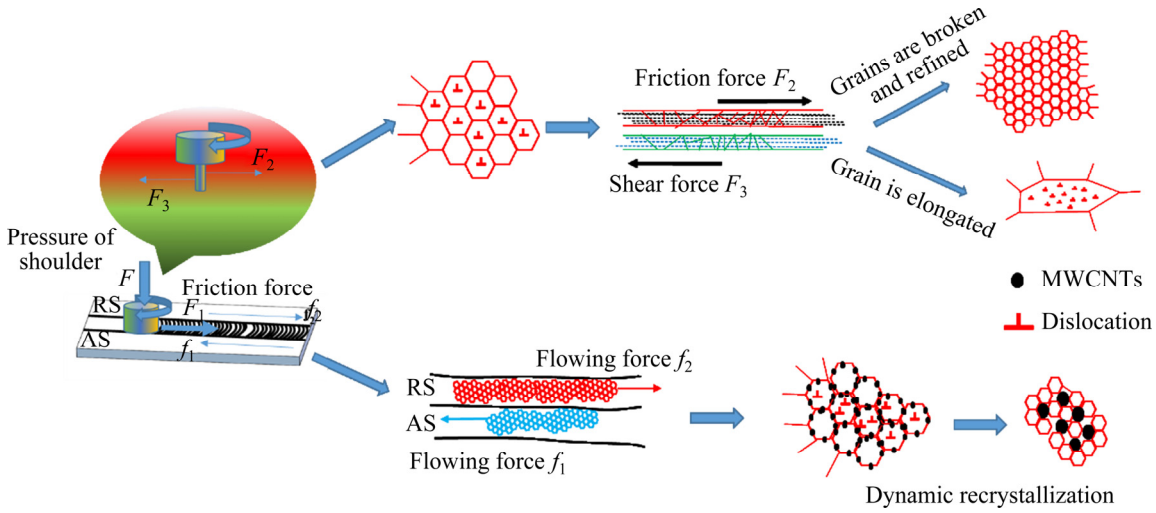

Fig. 14 Model diagram of grain refinement mechanism

are broken and refined more severely. In addition, because FSP has an advancing side and a receding side, the material undergoes plastic flow during the processing. When the material flows from the advancing side to the receding side, there are two flowing forces f_1 and f_2 between them, which causes the grain friction against each other and elongating. The heat generated by friction provides energy for the dynamic recrystallization. During FSP, the MWCNTs are uniformly dispersed in the matrix alloy, providing the nucleation particles when the matrix alloy undergoes dynamic recrystallization, resulting in refined recrystallized grains.

Although FSP is a kind of severe plastic deformation processing, it does not produce a large number of dislocations in the material. This can be attributed to the large amount of heat generated during FSP, which causes the dislocations annihilation [16]. Equation (1) can be used to estimate the temperature generated by FSP [34]. Accordingly, the temperature in the FSP in this work is as high as 460 °C. The high temperature makes the grains grow and coarsen, and makes the dislocations be annihilated. Therefore, the dislocation density in Samples 3 and 4 is relatively low, as shown in Figs. 8(a, b).

$$T=K\left(\frac{\omega^2}{10^4 V}\right)^{\alpha} T_{\mathrm{m}} \tag{1}$$

where T_{m}, ω and V are the melting point, rotation speed and forward speed, respectively, and α and K are constants, which can be estimated to be about 0.04 and 0.8 in Mg alloys, respectively [34].

After FSP+CR, the grains are further refined and some ultra-fine grains are found in the composite, as shown in Fig. 8(f). In addition, a large number of dislocations are found in the composite after CR, and the dislocation density is higher, as shown in Fig. 8(c). The heat generated in the CR process is much lower than that in FSP, which is not sufficient to cause grain growth and dislocation annihilation. Sample 5 has finer grains and has a higher dislocation density than Samples 3 and 4, resulting in the highest strength among all samples.

Additionally, CR makes the distribution of MWCNTs more uniform in the matrix alloy. From Fig. 6(c), MWCNTs agglomerate seriously in the stirring zone, which leads to the lower strength of Sample 4, compared with Sample 5. According to the shear hysteresis theory, load transfer occurs at the interface between matrix alloy and reinforcement through the shear stress, which increases the strength [35]. Therefore, in this composite, when an external force is applied, it will be transferred from the matrix alloy to the MWCNTs, thereby increasing the strength.

Usually, under severe plastic deformation, a significant increase in strength often brings about a decrease in the plasticity. However, in this work, the strength and plasticity of the samples are both improved, as shown in Fig. 12. This can be explained by the effect of MWCNTs. After cold rolling, the distribution of MWCNTs in the matrix alloy is more uniform, as shown in Fig. 6(d). The uniformly distributed MWCNTs hinder the

movement of dislocations during CR, which leads to the accumulation of dislocations, thus increasing the strength. In addition, due to the further reduction in grain size, a large number of grain boundaries are introduced, and the grain boundaries impede the movement of dislocations, leading to dislocation pile-ups, which generates large-range back stresses and local strain concentrations in the matrix alloy [36−38]. Figure 7 illustrates the mixed layered structure of MWCNTs and grains in the composite. The strain concentrations are usually located at the interlayer interface [9]. The strength and stiffness of MWCNTs are high enough to endure the high local stress caused by dislocation pile-ups and prevent further deformation of grains in the matrix alloy. Thus, MWCNTs limit the deformation of the matrix alloy and prevent crack formation. As the stress increases, the dislocations slip again into the other grains, and plastic deformation continues. In addition, an appropriate wide grain size distribution is also conducive to uniform deformation: coarse grains can increase ductility, and fine grains can increase strength [39,40]. In Figs. 6(d) and 7, a large number of fine grains and coarse grains are observed, showing a bimodal distribution. Many ultra-fine grains are found, as shown in Fig. 8(f). Therefore, the strength and plasticity of the composites can be improved after cold rolling.

5 Conclusions

(1) The MWCNTs/LA141 composite was successfully prepared by EPD, FSP and CR. The grains of matrix alloy are refined from 280 to 7 μm, along with some ultrafine grains.

(2) The yield strength and ultimate tensile strength of the composite are 259 and 313 MPa. Compared with the as-cast matrix alloy, the increments are 135.45% and 115.86%, respectively.

(3) The heat generated during FSP and the addition of MWCNTs promote the dynamic recrystallization and annihilate dislocations. The increase in strength during the FSP stage is mainly attributed to the grain refinement strengthening and the load transfer of MWCNTs. The heat generated from CR is not enough to annihilate dislocations. Therefore, the increase in strength in the CR stage is mainly attributed to grain the refinement strengthening, dislocation strengthening, and load transfer strengthening.

(4) A specific strength of 221.98 kN·m/kg is obtained in the composite, which is higher than that of many other metal matrix composites and alloys in literature.

Acknowledgments

This work was supported by the National Natural Science Foundation of China (Nos. 51871068, 51971071, 52011530025, and U21A2049), the National Key Research and Development Program of China (No. 2021YFE0103200), the Zhejiang Province Key Research and Development Program, China (No. 2021C01086), and the Fundamental Research Funds for the Central Universities, China (No. 3072021CFT1010).

References

[1] MA Xiao-chun, JIN Si-yuan, WU Rui-zhi. Corrosion behavior of Mg−Li alloys: A review [J]. Transactions of Nonferrous Metals Society of China, 2021, 31: 3228−3254. Doi: 10.1016/S1003-6326(21)65728-X.

[2] SUN Yue-hua, WANG Ri-chun, PENG Chao-qun, FENG Yan, YANG Ming. Recent progress in Mg−Li matrix composites [J]. Transactions of Nonferrous Metals Society of China, 2019, 29(1): 1−14. Doi:10.1016/S1003-6326(18)64909-X.

[3] JI Qing, ZHANG Shun, WU Rui-zhi, JIN Si-yuan, ZHANG Jing-huai, HOU Le-gan. High strength BCC magnesium−lithium alloy processed by cryogenic rolling and room temperature rolling and its strengthening mechanisms [J]. Materials Characterization, 2022, 187: 111869. Doi:10.1016/j.matchar.2022.111869.

[4] WANG Dan, LIU Shu-juan, WU Rui-zhi, ZHANG Shun, WANG Yang, WU Hua-jie, ZHANG Jing-huai, HOU Le-gan. Synergistically improved damping, elastic modulus and mechanical properties of rolled Mg−8Li−4Y−2Er−2Zn−0.6Zr alloy with twins and long-period stacking ordered phase [J]. Journal of Alloys and Compounds, 2021, 881: 160663. Doi:10.1016/j.jallcom.2021.160663.

[5] WANG Jia-hao, XU Lin, WU Rui-zhi, FENG Jing, HOU Le-gan, ZHANG Mi-lin. Enhanced electromagnetic interference shielding in a duplex-phase Mg−9Li−3Al−1Zn alloy processed by accumulative roll bonding [J]. Acta Metallurgica Sinica (English Letters), 2020, 33(4): 490−499. Doi:10.1007/s40195-020-01017-z.

[6] JIN Si-yuan, MA Xiao-chun, WU Rui-zhi, LI Ting-qu, WANG Jia-xiu, KRIT B L, HOU Le-gan, ZHANG Jing-huai, WANG Gui-xiang. Effect of carbonate additive on the microstructure and corrosion resistance of plasma electrolytic oxidation coating on Mg−9Li−3Al alloy [J]. International Journal of Minerals, Metallurgy and Materials, 2022, 29(7): 1453−1463. https://doi.org/10.1007/s12613-021-2377-0.

[7] WU Horng-yu, GAO Zhen-wei, LIN Jia-yu, CHIU Chui-hung. Effects of minor scandium addition on the properties of Mg−Li−Al−Zn alloy [J]. Journal of Alloys and Compounds, 2009, 474(1/2): 158−163. Doi:10.1016/j.jallcom.2008.06.145.

[8] GHAZANLOU S L, EGHBALI B, PETROV R. EBSD characterization of Al7075/graphene nanoplates/carbon nanotubes composites processed through post-deformation annealing [J]. Transactions of Nonferrous Metals Society of China, 2021, 31(8): 2250−2263. Doi:10.1016/S1003-6326(21)65652-2.

[9] SONG Zheng-xiang, HU Xiao-shi, XIANG Ye-yang, WU Kun, WANG Xiao-jun. Enhanced mechanical properties of CNTs/Mg biomimetic laminated composites [J]. Materials Science and Engineering A, 2021, 802: 140632. Doi:10.1016/j.msea.2020.140632.

[10] ZHAO Yong-hao, LIU Ji-zi, TOPPING Troy D, LAVERNIA ENRIQUE J. Precipitation and aging phenomena in an ultrafine grained Al-Zn alloy by severe plastic deformation [J]. Journal of Alloys and Compounds, 2021, 851: 156931. Doi:10.1016/j.jallcom.2020.156931.

[11] NOURI Z, TAGHIABADI R. Tribological properties improvement of conventionally-cast Al−8.5Fe−1.3V−1.7Si alloy by multi-pass friction stir processing [J]. Transactions of Nonferrous Metals Society of China, 2021, 31(5): 1262−1275. Doi: 10.1016/S1003-6326(21)65576-0.

[12] LIDDICOAT P V, LIAO X Z, ZHAO Y H, ZHU Y T, MURASHKIN M Y, LAVERNIA E J, VALIEV R Z, RINGER S P. Nanostructural hierarchy increases the strength of aluminium alloys [J]. Nature Communications, 2010, 1: 63. Doi:10.1038/ncomms1062.

[13] KE Li-ming, HUANG Chun-ping, XING Li, HUANG Ke-hui. Al−Ni intermetallic composites produced in situ by friction stir processing [J]. Journal of Alloys and Compounds, 2010, 503(2): 494−499. Doi:10.1016/j.jallcom.2010.05.040.

[14] RAJABI F, TAGHIABADI R, SHAERI M H. Tribological behavior of friction stir processed SiP/ZA40 in-situ composites [J]. Transactions of Nonferrous Metals Society of China, 2020, 30(11): 3043−3057. Doi:10.1016/S1003-6326(20)65441-3.

[15] KULITSKIY V, MALOPHEYEV S, MIRONOV S, KAIBYSHEV R. Grain refinement in an Al−Mg−Sc alloy: Equal channel angular pressing versus friction-stir processing [J]. Materials Science and Engineering A, 2016, 674: 480−490. Doi:10.1016/j.msea.2016.08.021.

[16] CHENG W, LIU C Y, GE Z J. Optimizing the mechanical properties of Al−Si alloys through friction stir processing and rolling [J]. Materials Science and Engineering A, 2021, 804：140786. Doi:10.1016/j.msea.2021.140786.

[17] YANG Kang, LI Wen-ya, NIU Peng-liang, YANG Xia-wei, XU Ya-xin. Cold sprayed AA2024/Al_2O_3 metal matrix composites improved by friction stir processing: Microstructure characterization, mechanical performance and strengthening mechanisms [J]. Journal of Alloys and Compounds, 2018, 736: 115−123. Doi:10.1016/j.jallcom.2017.11.132.

[18] ZHANG Shuai, CHEN Gao-qiang, WEI Jin-quan, LIU Yi-jun, XIE Rui-shan, LIU Qu, ZENG Shen-bo, ZHANG Gong, SHI Qing-yu. Effects of energy input during friction stir processing on microstructures and mechanical properties of aluminum/carbon nanotubes nanocomposites [J]. Journal of Alloys and Compounds, 2019, 798: 523−530. Doi:10.1016/j.jallcom.2019.05.269.

[19] RAHSEPAR M, JARAHIMOGHADAM H. The influence of multipass friction stir processing on the corrosion behavior and mechanical properties of zircon-reinforced Al metal matrix composites [J]. Materials Science and Engineering A, 2016, 671: 214−220. Doi:10.1016/j.msea.2016.05.056.

[20] GOH C S, WEI J, LEE L C, GUPTA M. Development of novel carbon nanotube reinforced magnesium nano-nanocomposites using the powder metallurgy technique [J]. Nanotechnology, 2006, 17(1): 7−12. Doi:10.1088/0957-4484/17/1/002.

[21] ALAVI NIA A, NOURBAKHSH S H. Microstructure and mechanical properties of AZ31/SiC and AZ31/CNT composites produced by friction stir processing [J]. Transactions of the Indian Institute of Metals, 2016, 69(7): 1435−1442. Doi:10.1007/s12666-015-0702-x.

[22] HUANG Yong-xian, LI Jun-chen, WAN Long, MENG Xiang-chen, XIE Yu-ming. Strengthening and toughening mechanisms of CNTs/Mg-6Zn composites via friction stir processing [J]. Materials Science and Engineering A, 2018, 732: 205−211. Doi:10.1016/j.msea.2018.07.011.

[23] KHODABAKHSHI F, GERLICH A P, ŠVEC P. Reactive friction-stir processing of an Al−Mg alloy with introducing multi-walled carbon nano-tubes (MW-CNTs): Microstructural characteristics and mechanical properties [J]. Materials Characterization, 2017, 131: 359−373. doi:10.1016/j.matchar. 2017.07.027.

[24] JAIN V K S, YAZAR K U, MUTHUKUMARAN S. Development and characterization of Al5083-CNTs/SiC composites via friction stir processing [J]. Journal of Alloys and Compounds, 2019, 798: 82−92. Doi:10.1016/j.jallcom.2019.05.232.

[25] LIU Gang, MA Zhen-dou, WEI Guo-bing, PENG Xiao-dong. Microstructure, tensile properties and corrosion behavior of friction stir processed Mg−9Li−1Zn alloy [J]. Journal of Materials Processing Technology, 2019, 267: 393−402. Doi:10.1016/j.jmatprotec.2018.12.026.

[26] CHEN Xiao-yang, ZHANG Yang, CONG Meng-qi. Effect of friction stir processing on microstructure and tensile properties of as-cast Mg−8Li−3Al−2Sn (wt.%) alloy [J]. Vacuum, 2020, 175: 109292. Doi: 10.1016/j.vacuum.2020.109292.

[27] XU Nan, FENG Ruo-nan, SONG Qi-ning, ZHAO Jian-hua, BAO Ye-feng. Influence of heterogeneous microstructures on the mechanical properties of low-temperature friction stir processed AZ91D Mg alloy [J]. Materials Science and Engineering A, 2021, 809: 141004. Doi:10.1016/j.msea.2021.141004.

[28] DARRAS B, KISHTA E. Submerged friction stir processing of AZ31 magnesium alloy [J]. Materials & Design, 2013, 47: 133−137. Doi:10.1016/j.matdes.2012.12.026.

[29] DEL VALLE J A, REY P, GESTO D, VERDERA D, JIMENEZ J A, RUANO O A. Mechanical properties of ultra-fine grained AZ91 magnesium alloy processed by friction stir processing [J]. Materials Science and Engineering A, 2015, 628(25): 198−206. Doi:10.1016/j.msea.2015.01.030.

[30] SHARAHI H J, POURANVARI M, MOVAHEDI M. Strengthening and ductilization mechanisms of friction stir processed cast Mg−Al−Zn alloy [J]. Materials Science and Engineering A, 2020, 781: 139249. Doi:10.1016/j.msea.2020.139249.

[31] NASIRI Z, KHORRAMI M S, MIRZADEH H, EMAMY M. Enhanced mechanical properties of as-cast Mg−Al−Ca magnesium alloys by friction stir processing [J]. Materials Letters, 2021, 296: 129880. Doi:10.1016/j.matlet.2021.129880.

[32] EIVANI A R, MEHDIZADE M, CHABOK S, ZHOU J. Applying multi-pass friction stir processing to refine the microstructure and enhance the strength, ductility and corrosion resistance of WE43 magnesium alloy [J]. Journal of Materials Research and Technology, 2021, 12: 1946−1957. Doi:10.1016/j.jmrt.2021.03.021.

[33] LUO X C, KANG L M, LIU H L, LI Z J, LIU Y F, ZHANG D T, CHEN D L. Enhancing mechanical properties of AZ61 magnesium alloy via friction stir processing: Effect of processing parameters [J]. Materials Science and Engineering A, 2020, 797: 139945. Doi:10.1016/j.msea.2020.139945.

[34] MISHRA R S, MA Z Y. Friction stir welding and processing [J]. Materials Science and Engineering R, 2005, 50(1/2): 1−78. Doi:10.1016/j.mser.2005.07.001.

[35] TROJANOVÁ Z, DROZD Z, KUDELA S, SZÁRAZ Z, LUKÁC P. Strengthening in Mg−Li matrix composites [J]. Composites Science and Technology, 2007, 67(9): 1965−1973. Doi:10.1016/j.compscitech.2006.10.007.

[36] WANG Wen, HAN Peng, PENG Pai, ZHANG Ting, LIU Qiang, YUAN Sheng-nan, HUANG Li-ying, YU Hai-liang, QIAO Ke, WANG Kuai-she. Friction stir processing of magnesium alloys: A review [J]. Acta Metallurgica Sinica (English Letters), 2020: 33(1): 43−57. Doi:10.1007/s40195-019-00971-7.

[37] WU X L, JIANG P, CHEN L, ZHANG J F, YUAN F P, ZHU Y T. Synergetic strengthening by gradient structure [J], Materials Research Letters, 2014, 2(4): 185−191. Doi:10.1080/21663831.2014.935821.

[38] MA X L, HUANG C X, XU W Z, ZHOU H, WU X L, ZHU Y T. Strain hardening and ductility in a coarse-grain/nanostructure laminate material [J]. Scripta Materialia, 2015, 103: 57−60. Doi:10.1016/j.scriptamat.2015.03.006.

[39] KOCH C C. Optimization of strength and ductility in nanocrystalline and ultrafine grained metals [J]. Scripta Materialia, 2003, 49(7): 657−662. Doi:10.1016/s1359-6462(03)00394-4.

[40] BIKKINA V, ALASILA S R, ADEPU K. Characterization of aluminum based functionally graded composites developed via friction stir processing [J]. Transactions of Nonferrous Metals Society of China, 2020, 30(7): 1743−1755. Doi: 10.1016/S1003-6326(20)65335-3.

电泳沉积、搅拌摩擦加工和冷轧制备高比强度 MWCNTs/Mg−14Li−1Al 复合材料

徐 林[1]，王佳豪[1]，巫瑞智[1,2]，张春波[3]，武华杰[1]，侯乐千[1]，张景怀[1]

1. 哈尔滨工程大学 超轻材料与表面技术教育部重点实验室，哈尔滨 150001；
2. 黑河学院 理学院，黑河 164300；
3. 哈尔滨焊接研究院有限公司，哈尔滨 150001

摘 要：采用电泳沉积技术、搅拌摩擦加工和冷轧工艺制备多壁碳纳米管增强 Mg−14Li−1Al 复合材料(MWCNTs/Mg−14Li−1Al)，研究复合材料的显微组织和力学性能。结果表明，该复合材料的显微硬度可达 HV 84.4，比铸态基体合金(HV 44.1)提高了 91.38%；其屈服强度和极限抗拉强度分别为 259 MPa 和 313 MPa，分别比铸态基体合金提高了 135.45%和 115.86%，比强度高达 221.98 kN·m/kg。MWCNTs 在搅拌摩擦加工和冷轧过程中作为形核颗粒，引起动态再结晶和晶粒细化。此外，MWCNTs 的加入可以阻碍位错运动和传递基体载荷，从而提高合金的强度。

关键词：金属基复合材料；镁锂合金；多壁碳纳米管；电泳沉积；搅拌摩擦加工；轧制；强化机制

(Edited by Xiang-qun LI)